Vesiculation in magmas from Stromboli and implications for normal Strombolian activity and paroxysmal explosions in basaltic systems

[*, 1)]Margherita Polacci, [2,3)]Don R. Baker, [4)]Lucia Mancini, [5)]Stefano Favretto, [6)]Reghan J. Hill

1) Istituto Nazionale di Geofisica e Vulcanologia, sezione di Catania, Piazza Roma 2, 95125 Catania, Italy

2) Earth and Planetary Sciences, GEOTOP-UQAM-McGill Research Centre, McGill University, 3450 rue University, Montreal, QC Canada H3A 2A7

3) Istituto Nazionale di Geofisica e Vulcanologia, sezione di Sismologia e Tettonofisica, via di Vigna Murata 605, 00143 Roma, Italy

4) SYRMEP Group, Sincrotrone Trieste S.C.p.A., S.S. 14, km 163,5 in Area Science Park, 34012 Basovizza (Trieste), Italy

5) Dipartimento Materiali e Risorse Naturali, Università di Trieste, via Valerio 2, 34127 Trieste, Italy

6) Department of Chemical Engineering, McGill University, 3610 University Street, Montreal, QC Canada H3A 2B2

*corresponding author; now at Istituto Nazionale di Geofisica e Vulcanologia, sezione di Pisa, via della Faggiola 32, 56126 Pisa, Italy, email: polacci@pi.ingv.it

Abstract

We performed a series of X-ray tomographic experiments and lattice Boltzmann permeability simulations on pyroclastic products from explosive activity at Stromboli between December 2004 and May 2006. We reconstructed the 3-D textures of vesicles to investigate the relationship between the nature of vesiculation in the erupted products and the dynamics of gas transport in the shallow conduit in order to derive implications for the eruptive behaviour of basaltic volcanoes. Scoriae from normal Strombolian explosions display remarkably consistent vesicle volume distributions fit by power-laws with an exponent of 1 (±0.2). We ascribe the origin of such distributions to the combined effect of coalescence and continuous nucleation events in the steady-state, shallow magma system that supplies normal Strombolian activity. Volume distributions and textures of vesicles in pumice clasts from the 5 April 2003 and 15 March 2007 paroxysmal activity are markedly different from those in the scoriae. Besides a power-law function with a higher exponent, portions of these distributions can be also fit by an exponential function, suggesting the attempt of the system to reach near-equilibrium conditions. The investigated pumice clasts also lack the large, connecting vesicles responsible for the development of degassing pathways in the Stromboli magma that erupts the scoriae. This testifies to a decreased degassing efficiency of the magma associated with paroxysmal explosions and potential overpressure build-up at depth. By comparison with degassing experiments on basaltic melts, we derive a time constraint on the order of minutes to hours for the incubation of paroxysms at Stromboli.

Keywords: basaltic explosions, vesicle textures, third dimension, permeability

Introduction

Volatiles play a significant role in magmatic systems and provide the driving force for volcanic eruptions. Because exsolved volatiles are recorded in volcanic rocks as vesicles (gas filled cavities), investigations of the nature of vesiculation in eruptive products is a tool for reconstructing the mechanisms of volatile exsolution and degassing in volcanic conduits. These mechanisms are not directly observable at the surface and consequently not easy to understand unambiguously from geophysical signals and geochemical studies of the gases emitted from active volcanoes. Although volcanic ejecta are imperfect records of magma chamber processes because of possible syn- and post-eruptive modification, research in the past 15 years has demonstrated that textures preserved in products from both effusive and explosive activity provide information on a number of processes occurring in conduits and at the surface. In particular, vesicles proved useful in the investigation of: i) the dynamics of magma ascent and fragmentation in both silicic [*Klug and Cashman*, 1994, 1996; *Klug et al.*, 2002; *Polacci et al.*, 2001, 2003; *Gurioli et al.*, 2005; *Polacci et al.*, 2005; *Adams et al.*, 2006; *Piochi et al.*, 2008] and mafic Plinian eruptions [*Sable et al.*, 2006]; ii) the development of magma permeability [*Klug and Cashman*, 1996; *Rust and Cashman*, 2004; *Mueller et al.*, 2005]; iii) the deformation history of magmas [*Polacci and Papale*, 1997; *Rust et al.*, 2003; *Manga*, 2005], and iv) rheological transitions [*Polacci et al.*, 1999], as well as surface degassing in active [*Cashman et al.*, 1994] and solidified [*Gaonac'h et al.*, 1996a] lava flows. With the exception of the pioneering work by *Mangan and Cashman* [1996], only very recently have vesicle textures been used to shed light on mechanisms driving basaltic explosive eruptions of mild to moderate intensity.

Large vesicles in scoria clasts from low energy Strombolian explosions have been found to record permeable pathways for gas flow in basaltic systems [*Polacci et al.*, 2007]. This type of vesicle has been used to highlight the role of gas percolation during passive degassing of persistently active volcanoes [*Burton et al.*, 2007a]. Heterogeneous vesicle textures and size distributions are found to accompany variations in the style of activity at Etna [*Polacci et al.*, 2006], Stromboli [*Lautze and Houghton*, 2007] and Villarrica (Chile) volcanoes [*Gurioli et al.*, 2008]. Here we study the textures of vesicles in fresh ejecta from Stromboli with the goal of investigating their relationships to, and implications for, the eruptive behaviour of this volcano. We report a series of synchrotron-based, high-resolution, X-ray tomographic experiments carried out on samples of scoria and pumice from normal and paroxysmal activity at Stromboli. These experiments allowed us to reconstruct digital volumes of the collected samples, visualize their 3-D inner structure, and determine the true vesicle size distribution, number density, and total vesicularity. In addition to this textural analysis, we performed lattice Boltzmann fluid flow simulations on selected tomographic volumes from our Stromboli sample suite. The simulations provide novel insights on the link between scoria and pumice structure and the dynamics of gas transport in basaltic magmas. This information, together with the textural dataset, significantly improves our understanding of the physics of degassing in basaltic systems.

Volcanological background and sample description

Stromboli volcano is known as the lighthouse of the Mediterranean Sea for its persistent activity that has been documented for the last 2000 years [Rosi et al., 2000]. The normal activity of the volcano consists of low to moderate energy, intermittent, Strombolian explosions from the summit craters located at 750 m asl (Fig.1), and of non-eruptive

degassing. The latter occurs as a continuous flow of passive, non-explosive gases supplied to the persistent volcano plume mainly by the open, summit vents, fractures and fumaroles present on the volcano flanks, and as a stream of more vigorous, discrete, non-passive gas puffs [*Harris and Ripepe*, 2007] associated with infrasonic pulses [*Ripepe et al.*, 1996]. Explosions at Stromboli result from the buoyant rise of deep-sourced gas slugs bursting at the magma free surface and occurring on average every 10-20 minutes [*Burton et al.*, 2007b]. They eject a mixture of volcanic gases and particles ranging in size from ash to scoria (lapilli, bombs and blocks) to heights of 100-200 m above the craters. Video camera systems (see weekly reports on Stromboli activity at the Istituto Nazionale di Geofisica e Vulcanologia, sezione di Catania (INGV-CT) website www.ct.ingv.it) and thermal imagery [*Patrick et al.*, 2007] of Stromboli have allowed scientists to refine previous classifications of its eruptive style [*Ripepe et al.*, 1993; *Chouet et al.*, 1999; *Ripepe and Marchetti*, 2002; *Chouet et al.*, 2003; *Marchetti and Ripepe*, 2005]. Explosions are subdivided into two main groups. The first group comprises events dominated by ejection of coarse ballistic particles. The second group is defined by explosions consisting of thick, ash-rich plumes; these latter events may exhibit gas thrust velocities and may be accompanied by the emission of coarser ejecta [*Patrick et al.*, 2007]. Both styles of eruptive behaviour are common at different craters [*Patrick et al.*, 2007], with events of the first group mostly associated with the North-East (NE) crater, and those of the second with the South-West (SW) crater [*Marchetti and Ripepe*, 2005].

Stromboli is also characterized by the less frequent occurrence of lava effusions and paroxysmal explosions [*Barberi et al.*, 1993]. Effusive activity at Stromboli consists of lava overflows from the summits craters or of lava flows erupted from vents located a

few hundred metres below the craters and emplaced in the Sciara del Fuoco, a horseshoe-shaped depression occupying the NW side of the volcano. Twenty-six lava effusions have been documented between 1888 and 2002, approximately one every 4 years [*Barberi et al.*, 1993; *Landi et al.*, 2006]. The most recent effusive episodes occurred during the 7-month-long flank activity of 2002-2003 [*Calvari et al.*, 2005; *Landi et al.*, 2006; *Lodato et al.*, 2007] and, recently, from 27 February to 2 April 2007 (see daily reports of the eruption activity at www.ct.ingv.it).

Paroxysms are of much higher explosivity in comparison to normal Strombolian events, posing a serious hazard for island residents and tourists [*Barberi et al.*, 1993; *Bertagnini et al.*, 1999]. They range from small-scale events [*Métrich et al.*, 2005], occurring at a rate of 1 to 3 per year in the last 10 years, during which showers of ash, lapilli and bombs blanketed the upper slopes of the volcano, to less frequent, large-scale paroxysms like the one of 1930 [*Imbò*, 1928; *Rittmann*, 1931]. During this event metre-sized bombs and blocks fell up to a few km away from the summit, affecting the two villages at the base of the volcano, Stromboli and Ginostra, and producing an almost continuous spatter deposit out to distal volcano areas [*Speranza et al.*, 2004]. The last paroxysms of 5 April 2003 and 15 March 2007 [*Calvari et al.*, 2006; *Rosi et al.*, 2006] had intensities between the paroxysmal end-members described above, and represent the most powerful explosive events that occurred at Stromboli in recent years.

Scoriae erupted during normal, explosive Strombolian activity, including those investigated in this study [*Corsaro and Miraglia*, 2006, 2007], and lava flows derive from a crystal-rich (40-50 vol%), volatile-poor, shoshonitic basalt magma that occupies the shallow (less than ~ 1 km below the craters) conduit [*Francalanci et al.*, 1999; *Métrich et al.*, 2001; *Francalanci et al.*, 2004; *Landi et al.*, 2004, *Corsaro et al.*, 2005;

Landi et al., 2006]. This degassed magma is thought to develop from decompression-induced, water-loss-driven, low-pressure crystallization of volatile-rich magma blobs rising from a deep plumbing system [*Métrich et al.,* 2001]. The deep magma is a crystal-poor, volatile-rich, high-potassium, calc-alkaline basalt only erupted during paroxysmal explosions. It generates the highly vesicular, crystal-poor pumice products characteristic of such activity at Stromboli [*Bonaccorso et al.,* 1996; *Bertagnini et al.*, 2003; *Métrich et al.*, 2005].

In this study we focus on the explosive activity that characterized the volcano from December 2004 to May 2006. During this period all three summit craters, NE, SW and Central (C), were active and occupied by one or more vents (Fig. 1) producing Strombolian explosions of varying intensity and style of activity. Samples of scoria were collected in the proximity of the source vent between minutes to a few hours after ejection during the activity of the 21 December 2004, 9 January 2005, 10 February 2005, 3 March 2005, 22 May 2005, 17 September 2005, 12 January 2006, 15 February 2006, 14 April 2006, 15 April 2006, 22 May 2006, 24 May 2006 and 25 May 2006. Our sample suite mostly comprises scoria of lapilli size, the only exception being the scoria bombs collected on 22 May 2005, and 14 and 15 April 2006. We mainly focus on lapilli because these samples do not exhibit textural features denoting post-eruptive degassing processes or cooling, such as bread-crusted surfaces, vesicularity gradients or groundmass crystallites, and therefore they are assumed to preserve evidence of the vesiculation state of the magma in the upper part of the conduit at the time they were erupted [*Mangan and Cashman,* 1996]. The deep-sourced, metre-sized bubbles that produce the explosive activity (i.e. the Strombolian bursts at the magma free surface) are never preserved in the erupted products, the only information about their nature coming from geochemical

[*Burton et al.*, 2007b] and geophysical [*Ripepe et al.*, 2007] determinations. However, the textures of lapilli-size scoria clasts provide valuable information on conditions of gas exsolution, transport and loss in the shallow conduit system feeding normal Strombolian activity. As we will demonstrate, significant textural differences exist between the lapilli produced during normal explosive activity and those produced during the paroxysmal activity of 5 April 2003 and 15 March 2007.

Summary of the explosive activity in 2005-2006

During the time span of our investigation, December 2004 to May 2006, Stromboli was marked by periods with significantly different eruptive behaviour (Fig. 2). In the following, we provide a brief synopsis of the eruptive activity that characterized our first (21 December 2004 - 17 September 2005) and second (12 January 2006 - 25 May 2006) sampling programs (Fig. 2). From December 2004 to the end of February 2005 the level of activity was high, as measured by the frequency per hour of the explosions and their height (check weekly reports at the INGV-CT website www.ct.ingv.it). One spectacular eruption in this sequence was on 9 January 2005, a high energy explosion with characteristics intermediate between normal and paroxysmal explosive activity [*Andronico et al.*, 2008]. From the end of February to the beginning of May the activity was low, but peaked again around 22 May. The activity decreased until early July 2005, followed by an increase up to early August when there was another high energy explosion on 6 August (for which we do not have samples). Stromboli returned to less explosive behaviour until the second half of September when the level of activity increased again until early October and our sampling program for year 2005 ended. During our second sampling program in 2006 the level of activity at Stromboli was

higher in comparison to our first period of sample collection (Fig. 2). An activity peak can be identified in January 2006, followed by a gradual decrease in activity between mid-January and mid-February and then an increase until the end of March. After a second peak in early April, the activity progressively decreased and remained low until the end of May 2006, when the second sample collection campaign terminated.

Methods

Analytical techniques and data reduction

Thirty-one (31) scoria clasts (from one to seven scoria clasts per sample suite erupted during the same day or explosion) and 6 pumice clasts (one from the 5 April 2003 paroxysmal explosion and 5 from the 15 March 2007 paroxysmal explosion) were selected on the basis of binocular microscope observation of their morphological features and vesicle content, and prepared for textural characterization via X-ray microtomography (μCT). Regretfully, the analysis of 1000's of samples (or thousands of cm^3 of samples) per day or explosion necessary for a statistically valid textural analysis is impossible by any current analytical technique. However, the samples chosen for tomography are to the best of our abilities representative of the complete sample suite collected for each day or explosion. Tomographic experiments were run at the SYRMEP beamline of the ELETTRA synchrotron radiation facility in Basovizza (Trieste, Italy), a third generation synchrotron source where it is possible to take advantage of the use of Phase-Contrast (PHC) imaging. While contrast in conventional X-ray imaging is generated only by the absorption properties of the sample, in PHC imaging contrast also arises from interference between parts of the wave front that have experienced different phase shifts (Fresnel diffraction). This technique allows us to visualize sample features

through the phase modifications that such features induce in the monochromatic transmitted X-ray beam [*Snigirev et al.,* 1995]. The important parameter in this approach is the sample-to-detector distance *d*. At *d~0* the recorded image is a conventional absorption radiograph. PHC μCT is simply obtained by locating the detector at a distance $d > 0$ (which typically varies from a few tens of centimetres to 1 metre) from the sample [*Cloetens et al.*, 1996]. The choice of *d* depends on the size *a* of the feature to be identified, measured perpendicularly to the beam direction, and on the X-ray wavelength (λ). In the edge detection regime ($d << a^2/\lambda$), images can be used qualitatively to extract morphological information from the sample.

A sketch of the experimental setup of the SYRMEP beamline is presented in Fig. 3a. During data acquisition, samples were mounted on a precision stage at a sample-to-detector distance of 20 cm, and rotated 180 degrees around an axis perpendicular to the monochromatic X-ray beam. The configuration used for each tomographic scan was a ring energy of 2.4 GeV, a beam energy between 27 and 33 keV, and a CCD field of view of 28.7 x 28.7 mm^2 or 18.0 x 12.0 mm^2, producing voxels (the 3-D equivalent of pixels) with edge lengths in each direction of 14 or 9 μm, respectively. This voxel size represents the minimum size vesicle we can detect. Projection images were recorded at 1/5 degree rotation steps by a detector system consisting of a 16 bit water-cooled CCD camera coupled to a Gadolinium oxysulphide scintillator by a straight fibre-optic coupler, and stored in a computer. The resulting 900 projections were reconstructed into tomographs via the backprojection algorithm with the creation of between 190 and 400 2-D image slices. The slices were stacked in the ImageJ software [*Abramoff et al.,* 2004] to produce digital volumes of the investigated scoriae in 3-D. These volumes were used for 3-D visualization of the internal structures of the scoria samples and for qualitative

characterization of scoria textures. In contrast to the acquisition of the tomographic images, which required a short time (<1 h), quantifying vesicle textures was time-consuming. Because on average it took from one to several days to process the vesicle population in each scoria clast, our quantitative characterization of vesicles focussed on scoriae erupted from December 2004 to September 2005, but also comprised two clasts from the normal explosive activity of 2006 (see Table 1).

In addition to the samples analyzed by the synchrotron source, pumice clasts from the 15 March 2007 paroxysmal event were processed at the Tomolab facility of ELETTRA (www.elettra.trieste.it/Labs/TOMOLAB). The Tomolab station is a cone-beam μCT system equipped with a sealed, micro-focus X-ray tube operating in an energy range from 40 to 130 kV (Fig. 3b). The CCD is a high resolution digital camera optically bonded to a tapered fibre-optic with a Gadolinium oxysulphide scintillator layer and provides a combination of a large field of view (approx. 50 x 33 mm^2) with voxels whose edge length is 12.5 μm. Exploiting the magnification effect offered by the cone-beam geometry [*Feldkamp et al.*, 1984; *Kak and Slaney*, 1987], the source-object-detector distance can be varied to achieve a spatial resolution close to the focal spot size of the source (5 μm) while imaging samples from a few millimetres to a few centimetres in size. Because the focal spot size is small enough, a limited but clearly detectable phase-contrast effect can be achieved [*Wilkins*, 1996], especially when low energies are used and object-to-detector distances are around 30 cm or larger. From the 12-bit tomographic projections acquired by the CCD camera during a 360° rotation of the sample, a set of at least 1024 2-D slices for each sample was reconstructed by the commercial Cobra Software Package Version 5, and imported into the ImageJ software to inspect the entire 3-D volume.

Individual vesicles within both scoria and pumice clasts were counted with the Blob3-D software [*Ketcham*, 2005] after segmentation by grey-scale thresholding and separation following two erosion and dilation steps. Several cycles of erosion and dilation were repeated on each sample for a number of different samples in order to optimize the separation procedure for these vesicular products. Vesicle volumes were measured with the same software and used together with bulk (i.e. the total volume investigated) and melt volumes (following *Proussevitch et al.* [2007]) to determine vesicle volume fractions and to plot vesicle volume distributions. Vesicle number densities, as the total number of vesicles normalized to either the bulk or the melt volume in each sample were also calculated. Textural parameters and vesicle volume distributions of the scoria and pumice clasts are reported in Table 1 and Figures 5 and 6.

Lattice Boltzmann simulations of fluid flow

To compare the permeability of scoria and pumice clasts, the permeability of samples 30305a1, 170905a, 170905c2, 240506b, Str50403 and Str150307 was investigated using lattice Boltzmann simulations of fluid flow [*Succi*, 2001; *Sukop and Thorne*, 2006]. The lattice Boltzmann technique treats the fluid as microscopic point particles that interact with each other and with the walls of the vesicles. This technique has been demonstrated to successfully reproduce macroscopic observations of fluid flow in porous media [*Succi*, 2001]. Because of computer limitations our simulations were performed using cropped central portions from each of the thresholded tomographic digital volumes. Despite the fact that the volumes investigated were small, these simulations allowed us to calculate and compare, for the first time, permeability values for scoria and pumice clasts from normal and paroxysmal explosive activity at Stromboli. The cropped volumes were cubes

with edge lengths in each of the three dimensions, arbitrarily labeled x, y and z, of between 140 and 180 pixels (the voxel size being either 14 x 14 x14 μm^3 or 9 x 9 x 9 μm^3, see previous section). The computations were performed with a code previously used by *Hill et al.* [e.g., 2001] for computing inertial flows in ordered and random arrays of impenetrable spheres. Accordingly, the software was modified to handle the complex vesicular geometry displayed in the X-ray tomographic images. Details of the lattice Boltzmann scheme implemented in this code are given by *Ladd* [1994 a, b]. In the referenced code the vesicles are fluid filled, and a uniform body force (equivalent to a uniform pressure gradient) is applied in a direction normal to one face of the domain. This force accelerates the fluid from rest until a steady state is reached in which the average pressure gradient balances the hydrodynamic drag. The time to reach steady state scales with the time it takes for momentum to traverse the largest vesicles in the domain. Our simulations reached a steady state, as indicated by the hydrodynamic force and momentum, in less than 30000 lattice Boltzmann time steps. From the average momentum flux and body force (average pressure gradient), we ascertained the Darcy permeability or, equivalently, the square of the Brinkman screening length [*Brinkman*, 1947]. Simulations were repeated with the force perpendicular to each of the three mutually orthogonal faces of the domain. In agreement, the permeabilities reported are the average values for these three mutually orthogonal directions. The complete simulation required approximately 5 days of computer time for each tomographic volume.

If the average pressure gradient is high enough, the lattice Boltzmann simulations permit the flow to enter a non-linear regime (after *Forchheimer* [1901]) in which the permeability, as measured by the ratio of the average flow rate and pressure gradient,

decreases with increasing microscale Reynolds number. Therefore, by varying the force over several orders of magnitude, we ensured that the permeabilities reported are indeed independent of the force and, therefore, are the Darcy permeabilities for creeping (inertialess) microscale flow. Accordingly, the flows from which we ascertained the reported permeabilities are steady and laminar, which is not the case at higher Reynolds numbers [e.g., *Hill and Koch*, 2002].

Results

Observations and measurements of 3-D vesicle textures

Tomographic images of lapilli-size scoria samples from the 2005 and 2006 normal explosive activity at Stromboli provide the unique ability to reconstruct and view the internal structure of these vesicular materials in 3-D. Fig. 4 provides examples of orthogonal views from two reconstructed scoria volumes. Observations of the 3-D volumes show that the vesicles range in volume from our minimum detection limit of 3 x 10^3 μm^3 to above 10^9 μm^3 and that vesicle textures can vary from one portion of a sample to another. These 3-D volumes allowed us to measure the total vesicularity, which varies from 0.24 to 0.78 in our sample set, and the number density, which is between 0.50 x 10^2 and 1.80 x 10^2 per mm^3 of bulk volume or 0.96 x10^2 and 4.55 x 10^2 per mm^3 of melt volume (Table 1). In addition, the 3-D volumes clearly demonstrate that the larger (>6 x 10^7 μm^3) vesicles were coalescing (i.e. forming a network of continuously connected vesicles) in the samples as they quenched and completely span the volume of the clast investigated (Fig. 4), as also discussed in *Polacci et al.* [2007]. This coalescence can only be unambiguously observed using the 3-D imagery from tomography, because many vesicles that appear unconnected in two-dimensional sections (e.g., a thin section) are

instead connected in the third dimension. The smallest vesicles are found in the septa and plateau regions between vesicles and in quenched glass between vesicles and crystals. After a given time these smallest vesicles would be expected either to coalesce with the larger ones around them or be incorporated into these latter by Ostwald ripening [*Baker et al.*, 2006], but the scoria clasts were erupted before this could occur. Finally, we note that crystals exert a significant control on the shapes and orientations of the medium-to-large vesicles (Fig. 4), but there is no clear evidence that vesicles nucleated on crystals or vice versa. Instead, it appears that growing vesicles pushed aside crystals.

The volume distributions of vesicles in scoria clasts from the 2005 and 2006 normal explosive activity at Stromboli are all remarkably similar, spanning the same wide range of volumes between ~ 10^4 to >10^9 μm^3 (Fig. 5). The vesicle size distribution of each scoria is clearly described by a power-law over the range of approximately 10^6 to 10^8 μm^3 with an exponent of 1 (±0.2), as shown in Fig. 5. Smaller vesicle volumes (<10^6 μm^3) can also be fit by power-laws, but with much lower exponents ranging from 0.3 to 0.5 (Fig. 5). All but one of the vesicle size distributions in the samples are characterized by a large vesicle with a volume of about one up to two orders of magnitude larger than the high end of the power-law distributions. The one distribution that does not contain the large vesicle, 100205a1 (Table 1, and Fig. 5g), is another sub-volume from the same clast as 100205a2 (Fig. 5h), which instead contains this vesicle type.

We concentrated our analysis on lapilli because they undergo limited or no post-eruptive processes. However, we processed one bomb sample (220505a, Table1) and found that it exhibits a power-law with a slightly lower exponent of 0.66 (Fig. 5p). The difference in the vesicle distribution of this clast, as compared to the lapilli samples, is seen in its depletion of vesicle volumes near 10^6 μm^3. This difference is attributed to the longer time

bombs take to cool after eruption, resulting in modifications of the vesicle size distribution through loss of some smaller vesicles, possibly by diffusive growth into larger vesicles, which, if carried to completion, is expected to lower the power-law exponent to near zero [*Gaonac'h et al.,* 1996a, b].

In contrast to the scoriae from normal Strombolian explosions, pumice samples from the paroxysmal explosions of 5 April 2003 and 15 March 2007 do not contain the large vesicle type described above (as highlighted in the 3-D reconstructions of Figs. 6a, c). These pumices display a population of small-to-medium sized spherical vesicles together with larger, ellipsoidal ones scattered throughout the sample. The vesicle volume distribution in each of these clasts is described by a poorly-fitted power-law with an exponent up to 1.40. In both pumice clasts the small-to-medium sized vesicles can also be fit with an exponential distribution (Figs. 6b, d). Measured vesicle number densities are 2.70×10^2 and 3.76×10^2 per mm^3 of bulk volume (or 6.43×10^2 and 8.60×10^2 per mm^3 of melt volume), and the vesicularity is 0.58 and 0.57 (Table 1).

Permeability simulations

The average of the permeabilities calculated from the lattice Boltzmann simulations in the three perpendicular directions of the scoria samples ranges from 2.0×10^{-10} to 7.3×10^{-10} m^2, whereas the pumice samples from the 5 April 2003 and 15 March 2007 paroxysmal eruptions have permeabilities of 2.1×10^{-11} m^2 and 8.6×10^{-11}, respectively (Table 2). The permeabilities calculated for each of the three directions display some differences, demonstrating the anisotropic characteristics and distributions of the vesicles in these porous rocks. In most cases the differences are small, and not large enough to be significant for this study, but one sample does display a 3 order of magnitude difference

(Table 2). The calculated permeabilities of the pumice samples are similar to those measured for pumice clasts of the 5 April 2003 paroxysm [*Mueller et al.*, 2008], supporting the use of lattice Boltzmann permeability simulations. In contrast to the pumice, the scoria samples are up to 2 orders of magnitude more permeable (Table 2).

Discussion

Implications of power-law distributions on normal Strombolian activity

The origin of power-law distributions in basaltic eruptive products has been discussed in a number of previous papers. The power-law exponent of 0.3 to 0.5 seen for smaller vesicles in some of our samples is well explained by the diffusive-growth theory of *Gaonac'h et al.* [1996 a, b]. Two main processes have been proposed to account for the distributions of the larger vesicles, greater than ~ 10^5 μm, that display exponents near 1. One process is that of steady-state vesicle growth through coalescence [*Gaonac'h et al.*, 1996a, b] (i.e. the process by which a network of connecting vesicles is formed that may span the whole volume under investigation), and the other is continuous nucleation of new vesicles [*Blower et al.*, 2001, 2002; *Yamada et al.*, 2005]. Indeed, recent degassing experiments at 1 atm using Stromboli basalt melts demonstrate that both coalescence and multiple nucleation events occurred in samples displaying power-law size distributions [*Bai et al.*, 2008]. There is no reason not to accept the presence of both mechanisms operating to produce the distributions observed in our natural samples.

The experiments of *Bai et al.* [2008] demonstrate that once coalescence and vesicle nucleation stop, the vesicle size distributions evolve from power-laws to exponential distributions in the space of minutes. The experiments of *Baker et al.* [2006] on the vesicle size distribution formed during decompression at 1200 ºC of a slightly water-

saturated albite melt demonstrated the same behaviour. Except, the timescale of evolution from a power-law to an exponential distribution was hours instead of minutes in the hydrous albite melt, which is orders of magnitude more viscous than the basaltic melt of *Bai et al.* [2008]. This evolution in the vesicle size distribution is associated with the transition of the system from far-from-equilibrium to near-equilibrium conditions, where the vesicles are all similar in size and approximately equidistant from each other, as seen in most foams of everyday life (e.g., beer, champagne, and soap). Because we do not see an exponential distribution in any of our Stromboli scoria samples from normal, Strombolian, explosive activity, we can infer that this transition never occurred and thus these scoriae were erupted at relatively far-from-equilibrium conditions. We ascribe the lack of such transition in our natural scoriae to the combination of coalescence and the occurrence of continuous vesiculation resulting in multiple nucleation events that affect the distribution of vesicles in the shallow conduit magma feeding the normal Strombolian activity (Fig. 5). We suggest that multiple nucleation events are recorded by the smallest vesicles located in the septa between larger vesicles and observed in scoria textures via our 3-D tomographic images (Fig. 4). We also think that a continuous vesicle nucleation process in the shallow Stromboli conduit is consistent with late-stage degassing of magma rich in halogens. This hypothesis is supported by the shallow-sourced, HCl-rich degassing signature of Stromboli [*Burton et al.*, 2007a] and by the relatively low pressure exsolution of HCl and HF reported for basaltic magmas [*Spilliaert et al.*, 2006].

The timescale of the evolution process from power-law to exponential distributions observed in the experiments of *Bai et al.* [2008] in a crystal-free system is only minutes, but in a natural system it may take longer. The relaxation times for diffusive- and viscosity-controlled vesicle growth were derived by *Navon et al.* [1998] and allow us to

make the necessary comparison between nature and experiments. The relaxation time for viscosity-controlled growth is the magma viscosity divided by the pressure difference between the vesicle and its surroundings. The melt viscosity for the *Bai et al.* [2008] experiments was 10 to 100 Pa s, whereas the bulk viscosity of the natural, crystal-rich, vesiculating Stromboli magma was estimated to be ~10 000 Pa s [*Burton et al.*, 2007a and references therein]. Therefore, providing the pressure differences are similar, the viscous relaxation time for the natural magma is estimated to be from 100 to 1000 times longer than in the experiments because the growing vesicles must viscously deform the melt+crystal mixture of the magma (as seen Fig. 4). The calculated relaxation time for diffusive vesicle growth in the scoriae, i.e., the ratio of the squared vesicle radius to the volatile diffusion coefficient of the melt, is also between approximately 100 to 1000 times longer than the experiments. Thus the ratio of the timescale in the natural system to that in the experiments of *Bai et al.* [2008] is at least 100, irrespective of whether growth is diffusive- or viscosity-controlled. Applying this factor to the observed timescales of the experiments indicates that the natural system may take as long as hours for the vesicle size distributions to evolve from power-law to exponential size distributions. Thus, the vesicles in the scoria samples from normal Strombolian activity displaying a power-law size distribution did not experience conditions that allowed them to relax to near-equilibrium distributions for any longer than minutes to hours before eruption.

Correlation of textural measurements with explosive activity

The scoriae from normal Strombolian activity (discussed above) are remarkable for their consistency in vesicle size distributions, suggesting steady-state conditions for the shallow magma system that supplies the explosions. Although Stromboli is known for the

persistency of its activity during at least the past 2000 years, the intensity as well as the style of the normal explosions varies with time (see Fig. 2). To investigate if changes in the eruptive activity correlate with textures of the erupted scoriae we consider the continuous 9-month-long record of vesicle measurements that we have for samples collected between 21 December 2004 and 17 September 2005.

Despite variations in activity during the time of our study, and with the exception of the 9 January 2005 high energy explosion, we did not find any clear relationships between the intensity of normal Strombolian explosions and either the vesicularity or vesicle number density of the ejected material (Fig. 7). For example, periods of high-level activity in terms of explosion frequency and height are associated with either more-vesicular scoria (i.e. 17 September 2005) or less-vesicular scoria (i.e. 10 February 2005). *Lautze and Houghton* [2007] observed a similar diversity of explosive activity at Stromboli in 2002 and explained it in terms of variations in the magma supply rate versus discharge rate, linking textures to the rheology of the more-or-less stagnant magma in the shallower part of the conduit. In our study we discovered that vesicularity and vesicle number density cannot be linked unambiguously to normal explosive activity at Stromboli, unless these parameters are interpreted in light of independent geochemical and geophysical measurements.

However, we did find that the vesicle number density increases with the eruption intensity from normal explosive activity through small-scale paroxysms up to paroxysmal explosions (Table 1). The largest explosion during this period of investigation, 9 January 2005, has the highest vesicle number density (Table 1). This correlation is consistent with observations made in products from the explosive activity of other persistently active basaltic volcanoes [*Polacci et al.*, 2006].

Implications of vesicle size distributions on paroxysmal explosions at Stromboli

The vesicle number densities of the pumice clasts from the 5 April 2003 and 15 March 2007 paroxysms are the largest (Table 1). This is consistent with the correlation between explosivity and vesicle number density that we observed when products from normal and high energy explosions are compared. Despite the consistency of the vesicle number densities with this trend, the vesicle size distributions of the pumice samples are markedly different.

The small-to-medium sized vesicles (Fig. 6) in both pumice samples from paroxysmal eruptions can be fit by an exponential function, implying vesiculation histories different from normal Stromboli scoria. We interpret these distributions to indicate the attempt of the system to reach near-equilibrium conditions that produce exponential distributions of vesicle volumes [*Bai et al.*, 2008]. It appears, however, that this attempt did not go to completion, because we see remnants of power-law behaviour but with a steeper exponent (Fig. 6b, d). Based on the comparison between experimental and natural samples, we previously calculated that the transition from a power-law to an exponential distribution may take minutes to hours to reach completion in nature. Therefore this transition may provide a time constraint on the triggering of paroxysmal explosions.

An additional difference between the pumice and scoria is that the pumice lacks the largest, coalescing, vesicle type connecting one side of the sample to the other (compare Figs. 4 and 6a, c). This large vesicle was found to play a fundamental role in promoting permeability development in the Stromboli shallow magmatic system and its degassing [*Polacci et al.*, 2007]. The efficiency of degassing is supported by measurements of persistent, passive degassing during periods of normal Strombolian behaviour [*Burton et*

al., 2007a]. In comparison, the lack of the largest, connecting vesicle in the pumice clasts testifies to the fact that such a vesicle type is not present in the deeper magma feeding paroxysmal explosions prior to these events. This observation leads us to the assumption that degassing conditions are less efficient in the deeper feeding system associated with paroxysmal activity. Indeed, permeabilities from lattice Boltzmann simulations support this observation. The permeability of the scoria clasts is from one to ~ two orders of magnitude higher than that of the pumice from the 5 April 2003 explosion, and about 3 times to one order of magnitude higher than that of the pumice from the 15 March 2007 explosion (Table 2). These differences are evident from the two visualizations of the simulations where the effect of the large, connecting vesicles on flow is readily seen (Fig. 8 and Electronic Supplementary Material).

Based upon these observations and inferences we propose the following scenario for normal Strombolian activity and for the events that lead to paroxysmal explosions. Under normal conditions there is a continuous pathway for gas and magma ascent from the deeper to the shallower part of the system; continuous vesicle nucleation and coalescence produce the power-law distributions and large, spanning vesicles that we find in the scoriae from the normal, daily explosions at Stromboli. Prior to a paroxysm, the efficiency of degassing in the deeper feeding system drops because only a few or no spanning vesicles are present and overpressure builds up at depth. This situation lasts until the overpressure exceeds the tensile strength of the shallower magma and the paroxysm occurs. It is notable that the vesicle textures observed in pumice clasts are consistent with initial sub-equilibrium vesiculation but then very fast magma ascent, a mechanism that agrees well with either of the two alternative hypotheses previously proposed to explain the dynamics of paroxysmal explosions at Stromboli: the fast ascent

of either deep, volatile-rich, magma blobs [*Bertagnini et al.*, 2003; *Metrich et al.*, 2005; *Polacci et al.*, 2006] or large gas pockets produced by intermittent bubble foam collapse [*Allard*, 2007].

Our analysis suggests that the incubation time for paroxysms is short, minutes to hours, implying that drastic changes in the Stromboli magmatic system occur rapidly. A further, independent piece of evidence for our proposed mechanism and its timescale is provided by decreases in the measured gas fluxes only hours before the paroxysm of 15 March 2007 (M.R. Burton, personal communication, 2008). We have not yet identified the causal event that results in the significant drop in degassing efficiency that leads to paroxysms. However, because paroxysms occur frequently, with a recurrence interval of one year, it seems that the precipitating event can occur easily.

Conclusions

The 3-D study of vesicle textures, vesicle size distributions and permeability in scoria and pumice clasts respectively from normal and paroxysmal explosions at Stromboli provides novel insights into the dynamics of vesiculation and degassing in basaltic magmas. Results from the investigation of vesicles in scoria clasts from normal explosive activity revealed that the shallow conduit magma supplying the daily explosions at Stromboli is a system operating under remarkable steady-state conditions. In contrast, pumice products from paroxysmal explosions display a markedly different vesiculation history implying that gas transport in the associated magma is also different. We propose that the lack of percolation pathways and lower permeabilities in pumice clasts compared to scoria clasts document a less efficient degassing occurring in the deeper magma feeding system prior to paroxysmal explosions. Although the incubation time of paroxysms is unknown,

vesiculation patterns indicate that it may be on the order of minutes to hours, demonstrating the necessity of real-time monitoring to detect any precursory activity in basaltic explosive systems. This information, if combined with results from independent geophysical and geochemical investigations, is expected to shed light on the mechanisms that trigger the inception of paroxysmal eruptions as well as on the transition between eruptive styles at Stromboli and other basaltic volcanoes characterized by a variety of eruptive behaviour.

Acknowledgements

This work was supported by the Istituto Nazionale di Geofisica e Vulcanologia and the Italian Civil Protection. We thank D. Andronico, M. Rosi, M. Ripepe and M. Zaia for sample collection and L. Bai, L. Colò, G. Tromba and F. Zanini for assistance during tomographic measurements. We are grateful to M. Pompilio, an anonymous reviewer and Associate Editor J. Weertman for their constructive reviews that greatly improved the paper. This work was also partially supported by an NSERC Discovery grant to D.R.B. and is GEOTOP contribution #2008-0022.

References

Abramoff, M. D., P. J. Magelhaes, and S. J. Ram (2004), Image Processing with ImageJ, *Biophot. Int.*, *11*, 36-42.

Adams, N. K., B. F. Houghton, S. A. Fagents, and W. Hildreth (2006), The transition from explosive to effusive eruptive regime: the example of the 1912 Novarupta eruption, Alaska, *Geol. Soc. Am. Bull.*, *118*, 620–634.

Allard, P. (2007), A CO_2-rich gas trigger of explosive paroxysms at Stromboli volcano (Italy), *Geophys. Res. Abstr., 9*, 08044.

Andronico, D., R. A. Corsaro, A. Cristaldi, and M. Polacci (2008), Characterizing high energy explosive eruptions at Stromboli volcano using multidisciplinary data: An example from the 9 January 2005 explosion, *J. Volcanol. Geotherm. Res.*, doi:10.1016/j.jvolgeores.2008.05.011

Bai, L., D. R. Baker, and M. Rivers (2007), Experimental Study of Bubble Growth in Stromboli Basalt Melts at 1 Atmosphere, *E. Planet. Sci. Lett., 267,* 533-547, doi: 10.1016/j.epsl.2007.11.063.

Baker, D.R., P. Lang, G. Robert, J.-F Bergevin, E. Allard, and L. Bai (2006), Bubble growth in slightly supersaturated albite melt at constant pressure, *Geochim. Cosmochim. Acta, 70*, 1821-1838.

Barberi, F., M. Rosi, and A. Sodi (1993), Volcanic hazard assessment at Stromboli based on review of historical data, *Acta Vulcanol., 3*, 173–187.

Bertagnini, A., M. Coltelli, P. Landi, M. Pompilio, and M. Rosi (1999), Violent explosions yield new insights into dynamics of Stromboli volcano, *Eos Trans AGU*, *80*(52), 633-636.

Bertagnini, A., N. Métrich, P. Landi, and M. Rosi (2003), Stromboli volcano (Aeolian Archipelago, Italy): An open window on the deep-feeding system of a steady state basaltic volcano, *J. Geophys. Res., 108*(B7), 2336, doi:10.1029/2002JB002146.

Blower, J. D., J. P. Keating, H. M. Mader, and J. C. Phillips (2001), Inferring volcanic degassing processes from vesicle size distributions, *Geophys. Res. Lett., 28*, 347–350, doi:10.1029/2000GL012188.

Blower, J. D., J. P. Keating, H. M. Mader, and J. C. Phillips (2002), The evolution of bubble size distributions in volcanic eruptions, *J. Volcanol. Geotherm. Res.*, *120*, 1–23.

Bonaccorso, A., C. Cardaci, M. Coltelli, P. Del Carlo, S. Falsaperla, S. Pannucci, M. Pompilio, and L. Villari (1996), Volcanic activity on Stromboli in 1993, *Bulletin of Volcanic eruptions- Supplement to Bull. Volc., 33*, 7-13.

Brinkman, H. C. (1947), A calculation of the viscous force exerted by a flowing fluid on a dense swarm of particles, *Appl. Sci. Res., A1*, 27-34.

Burton, M. R., H. M. Mader, and M. Polacci (2007a), The role of gas percolation in quiescent degassing of persistently active volcanoes, *E. Planet. Sci. Lett., 264*, 46-60.

Burton, M. R., P. Allard, F. Murè, and A. La Spina (2007b), Magmatic gas composition reveal the source depth of slug-driven Strombolian explosive activity, *Science, 317*, 227-230.

Calvari, S., S. Spampinato, L. Lodato, A. J. L. Harris, M. R. Patrick, J. Dehn, M. R. Burton, and D. Andronico (2005), Chronology and complex volcanic processes during the 2002–2003 flank eruption at Stromboli volcano (Italy) reconstructed from direct observations and surveys with a handheld thermal camera, *J. Geophys. Res., 110* (B02201), doi:10.1029/2004JB003129.

Calvari, S., L. Spampinato, and L. Lodato (2006), The 5 April 2003 vulcanian paroxysmal explosion at Stromboli volcano (Italy) from field observations and thermal data, *J. Volcanol. Geotherm. Res., 149*, 160-175.

Cashman, K. V., M. T. Mangan, and S. Newman (1994), Surface degassing and modifications to vesicle size distributions in Kilauea basalt, *J. Volcanol. Geotherm. Res., 61*, 45–68.

Chouet, B., G. Saccorotti, P. Dawson, M. Martini, R. Scarpa, G. De Luca, G. Milana, and M. Cattaneo (1999), Broadband measurements of the sources of explosions at Stromboli volcano, *Geophys. Res. Lett.*, *26*, 1937–1940.

Chouet, B., P. Dawson, T. Ohminato, M. Martini, G. Saccorotti, F. Giudicepietro, G. De Luca, G. Milana, and R. Scarpa (2003), Source mechanisms of explosions at Stromboli Volcano, Italy, determined from moment-tensor inversions of very-long-period data, *J Geophys Res*, *108*, doi:10.1029/2002JB001919.

Cloetens, P., R. Barrett, J. Baruchel, J.P. Guigay and M. Schlenker (1996), Phase objects in synchrotron radiation hard X-ray imaging, *J. Phys. D: Appl. Phys.*, *29*, 133-146.

Corsaro, R. A., L. Miraglia, and V. Zanon (2005), Petrologic monitoring of glasses in the pyroclastites erupted in February 2004 by the Stromboli volcano, Aeolian Islands, Southern Italy, *J. Volcanol. Geotherm. Res.*, *139*, 339-343.

Corsaro, R. A., and L. Miraglia (2006), Attività di monitoraggio petrologico Stromboli - II semestre 2005, Prot. int. n° UFVG2006/27, report, INGV-sezione di Catania, Italy.

Corsaro, R. A. and L. Miraglia (2007), Eruzione Stromboli 2007. Composizione dei vetri dei prodotti eruttati, Prot. Int. n° UFVG2007/015, report, INGV-sezione di Catania, Italy.

Forchheimer, P. (1901), Wasserbewegung durch Boden, *Z. Ver. Dtsch. Ing.*, *45*, 1781–1788.

Francalanci, L., S. Tommasini, S. Conticelli, and G. R. Davies (1999), Sr isotope evidence for short magma residence time for the 20th century activity at Stromboli volcano, Italy, *E. Planet. Sci. Lett.*, *167*, 61– 69.

Francalanci, L., S. Tommasini, and S. Conticelli (2004), The volcanic activity of Stromboli in the 1906–1998 AD period: mineralogical, geochemical and isotope data

relevant to the understanding of the plumbing system, *J. Volcanol. Geotherm, Res.*, *131*, 179–211.

Gaonac'h, H., S. Lovejoy, and J. Stix (1996a), Scaling effects on the bubble shape, size and heterogeneity of lavas from Mount Etna, *J. Volcanol. Geotherm. Res.*, *74*, 131-153.

Gaonac'h, H., S. Lovejoy, J. Stix, and D. Scherzter (1996b), A scaling growth model for bubbles in basaltic lava flows, *E. Planet. Sci. Lett.*, *139*, 395-409.

Gurioli, L., B. F. Houghton, K. V. Cashman, and R. Cioni (2005), Complex changes in eruption dynamics during the 79 AD eruption of Vesuvius, *Bull. Volcanol.*, *67*, 144-159.

Gurioli, L., A. J. L. Harris, B. F. Houghton, M. Polacci and M. Ripepe (2008), Textural and geophysical investigation of explosive basaltic activity at Villarrica volcano, in press, *J. Geophys. Res*.

Harris, A. J. L., and M. Ripepe (2007), Temperature and dynamics of degassing at Stromboli, *J. Geophys. Res.*, *112*, doi:10.1029/2006JB004393.

Hill, R. J., D. L. Koch, and A. J. C. Ladd (2001), The first effects of fluid inertia on flows in ordered and random arrays of spheres, *J. Fluid Mech*., *448*, 213-241.

Hill, R. J., and D. L. Koch (2002), Transition from steady to weakly turbulent flow in a close-packed ordered array of spheres, *J. Fluid. Mech.*, *465*, 59-97.

Ketcham, R.A. (2005), Computational methods for quantitative analysis of three-dimensional features in geological specimens, *Geosphere*, *1*, 32-41.

Klug, C., and K.V. Cashman (1994), Vesiculation of May 18, 1980, Mount St. Helens magma, *Geology*, *22*, 468–472.

Klug, C., and K. V. Cashman (1996), Permeability development in vesiculating magmas: implications for fragmentation, *Bull. Volcanol.*, *58*, 87–100.

Klug, C., K. V. Cashman, and C. R. Bacon (2002), Structure and physical characteristics of pumice from the climactic eruption of Mt Mazama (Crater Lake), Oregon, *Bull. Volcanol.*, *64*, 486–501.

Imbò, G. (1928), Parossismo di Stromboli nel Settembre 1930, *Bull. Volcanol.*, *15-18*, 177-185.

Ladd, A. J. C. (1994a), Numerical simulations of particulate suspension via a discretized Boltzmann equation. Part 1. Theoretical foundation, *J. Fluid Mech.*, *271*, 285-309.

Ladd, A. J. C. (1994b), Numerical simulations of particulate suspension via a discretized Boltzmann equation. Part 2. Numerical results, *J. Fluid Mech.*, *271*, 311-339.

Landi, P., N. Métrich, A. Bertagnini, and M. Rosi (2004), Dynamics of magma mixing and degassing recorded in plagioclase at Stromboli (Aeolian Archipelago, Italy), *Contrib. Mineral Petrol.*, *147*, 213– 237.

Landi, P., L. Francalanci, M. Pompilio, M. Rosi, R. A. Corsaro, C. M. Petrone, I. Nardini and L. Miraglia (2006), The December 2002–July 2003 effusive event at Stromboli volcano, Italy: Insights into the shallow plumbing system by petrochemical studies, *J. Volcanol. Geotherm. Res.*, *155*, 263-284.

Lautze, N. C., and B. F. Houghton (2007), Linking variable explosion style and magma textures during 2002 at Stromboli volcano, Italy, *Bull. Volcanol.*, 69, 445-460.

Lodato, L., L. Spampinato, A. Harris, S. Calvari, J. Dehn, and M. Patrick (2007), The morphology and evolution of the Stromboli 2002-2003 lava flow field: an example of a basaltic flow field emplaced on a steep slope, *Bull. Vulcanol.*, *69*, 661-679, doi:10.1007/s00445-006-0101-6.

Manga, M. (2005) Deformation of flow bands by bubbles and crystals, in *Kinematics and dynamics of lava flows*, edited by M Manga and G. Ventura, GSA Special Paper 396, pp. 47-54, doi:10.1130/2005.2396(04).

Mangan, M., and K. V. Cashman (1996), The structure of basaltic scoria and reticulite and inferences for vesiculation, foam formation, and fragmentation in lava fountains, *J. Volcanol. Geotherm. Res.*, *73*, 1–18.

Marchetti, E., and M. Ripepe (2005), Stability of the seismic source during effusive and explosive activity at Stromboli Volcano, *Geophys. Res. Lett.*, *32*, doi: 10.1029/2004GL021406.

Métrich, N., A. Bertagnini, P. Landi, and M. Rosi (2001), Crystallisation driven by decompression and water loss at Stromboli volcano (Aeolian Islands), *J. Petrol.*, *42*, 1471–1490.

Métrich, N., A. Bertagnini, P. Landi, M. Rosi, and O. Belhadj (2005), Triggering mechanism at the origin of paroxysms at Stromboli (Aeolian Archipelago, Italy): The 5 April 2003 eruption, *Geophys. Res. Lett*., *32*, doi:10.1029/2004GL022257.

Mueller, S., O. Melnik, O. Spieler, B. Scheu, and D. B. Dingwell (2005), Permeability and degassing of dome lavas undergoing rapid decompression: and experimental determination, *Bull. Volcanol.*, *67*, 526-538.

Mueller, S., B. Scheu, O. Spieler, and D. B. Dingwell (2008), Permeability control on magma fragmentation, *Geology*, *36*, 399-402.

Navon, O., A. Chekmir, and V. Lyakhovsky (1988), Bubble growth in highly viscous melts: Theory, experiments, and autoexplosivity of dome lavas, *E. Planet. Sci. Lett.*, *160*, 763-776, 1998.

Patrick, M. R., A. J. L. Harris, M. Ripepe, J. Dehn, D. A. Rothary, and S. Calvari, Strombolian explosive styles and source conditions: insights from thermal (FLIR) video (2007), *Bull. Volcanol., 69,* 769-784.

Piochi, M., M. Polacci, G. De Astis, A. Zanetti, A. Mangiacapra, R. Vannucci, and D. Giordano (2008), Texture and composition from pumices and scoriae of the Campi Flegrei caldera (Italy): implications on the dynamics of explosive eruptions, *Geochem. Geophys. Geosyst*, doi:10.1029/2007GC001746.

Polacci, M., and P. Papale (1997), The evolution of lava flows from ephemeral vents at Mount Etna: insights from vesicle distribution and morphological studies, *J. Volcanol. Geotherm. Res., 76*, 1–17.

Polacci, M., K. V. Cashman, and J. P. Kauahikaua (1999), Textural characterization of the pahoehoe–aa transition in Hawaiian basalt, *Bull. Volcanol., 60,* 595-609.

Polacci, M., P. Papale, and M. Rosi (2001), Textural heterogeneities in pumices from the climactic eruption of Mount Pinatubo, 15 June 1991, and implications for magma ascent dynamics, *Bull. Volcanol., 63*, 83–97.

Polacci, M., L. Pioli, M. Rosi (2003), The Plinian phase of the Campanian Ignimbrite eruption (Phlegrean Fields, Italy): evidence from density measurements and textural characterization of pumice, *Bull. Volcanol., 65*, 418-432.

Polacci, M., M. Rosi, P. Landi, A. Di Muro, and P. Papale (2005), Novel interpretation for shift between eruptive styles in some volcanoes, *Eos, 86*, 333-340.

Polacci, M., R. A. Corsaro, and D. Andronico (2006), Coupled textural and compositional characterization of basaltic scoria: insights into transition from Strombolian to fire-fountain activity at Mount Etna (Italy), *Geology, 34*, 201-204.

Polacci, M., D. R. Baker, L. Bai, and L. Mancini (2007), Large vesicles record pathways of degassing at basaltic volcanoes, *Bull. Volcanol.*, 10.1007/s00445-007-0184-8.

Proussevitch, A. A., D. L. Sahagian, and E. P. Tsentalovich (2007), Statistical analysis of bubble and crystal size distributions: Formulations and procedures, *J. Volcanol. Geotherm. Res.*, *164*, 95-111.

Ripepe, M., M. Rossi, and G. Saccorotti (1993), Image processing of explosive activity at Stromboli, J. Volcanol. Geotherm. Res., 54, 335–351.

Ripepe, M., P. Poggi, T. Braun, and E. Gordeev (1996), Infrasonic waves and volcanic tremor at Stromboli, *Geophys. Res. Lett.*, *23*(2), 181–184.

Ripepe, M., and E. Marchetti (2002), Array tracking of infrasonic sources at Stromboli volcano, *Geophys. Res. Lett.*, *29*, doi: 10.1029/2002GL015452.

Ripepe, M., E. Marchetti, and G. Ulivieri (2007), Infrasonic monitoring at Stromboli volcano during the 2003 effusive eruption: Insights on the explosive and degassing process of an open conduit system, *J. Geophys. Res.*, *112*, B09207, doi:10.1029/2006JB004613.

Rittmann, A. (1931), Der Ausbruch des Stromboli am 11 September 1930, *Zeits. Vulkanol.*, *14*, 47-77.

Rosi, M., A. Bertagnini, and P. Landi (2000), Onset of the persistent activity at Stromboli volcano (Italy), *Bull. Volcanol.*, *62*, 294-300.

M. Rosi, A. Bertagnini, A. J. L. Harris, L. Pioli, M. Pistolesi and M. Ripepe (2006), A case history of paroxysmal explosion at Stromboli: Timing and dynamics of the April 5, 2003 event, *E. Planet. Sci. Lett.*, *243*, 594-606.

Rust, A. C., M. Manga, and K. V. Cashman (2003), Determing flow type, shear rate and shear stress in magmas from bubble shapes and orientations, *J. Volcanol. Geotherm. Res.*, *2560*, 1-22.

Rust, A.C., and K.V. Cashman (2004), Permeability of vesicular silicic magma: inertial and hysteresis effects, *Earth Planet. Sci. Lett.*, *228*, 93-107.

Sable, J. E., B. F. Houghton, P. Del Carlo, and M. Coltelli (2006), Changing conditions of magma ascent and fragmentation during the Etna 122 BC basaltic Plinian eruption: Evidence from clast microtextures, *J. Volcanol. Geotherm. Res.*, *158*, 333-354.

Spilliaert, N., N. Métrich, and P. Allard (2006), S–Cl–F degassing pattern of water-rich alkali basalt: Modelling and relationship with eruption styles on Mount Etna volcano, *E. Planet. Sci. Lett.*, *248*, 772-786.

Snigirev, A., I. Snigireva, V. Kohn, S. Kuznetsov, and I. Schelokov (1995), On the possibilities of X-ray phase contrast imaging by coherent high energy synchrotron radiation, *Rev. Sci. Instr.*, *66*, 5486–5492.

Speranza, F., M. Pompilio, and L. Sagnotti (2004), Paleomagnetism of spatter lavas from Stromboli volcano (Aeolian Islands, Italy): Implications for the age of paroxysmal eruptions, *Geoph. Res. Lett.*, *31*, doi:10.1029/2003GL018944.

Succi, S. (2001), The lattice Boltzmann equation for fluid dynamics and beyond, 288 pp., Clarendon Press, Oxford.

Sukop, M. C., and D. T. Thorne, (2006), Lattice Boltzmann Modeling, an introduction for geoscientists and engineers, 172 pp, Springer, Berlin.

Yamada, K., H. Tanaka, K. Nakazawa, and H. Emori (2005), A new theory of bubble formation in magma, *J. Geophys. Res.*, *110*, doi:10.1029/2004JB003113.

Wilkins, S.V., T. E. Gureyev, D. Gao, A. Pogany, and A. W. Stevenson (1996), Phase-contrast imaging using polychromatic hard X-rays, *Nature, 384*, 335-338.

Figure Captions

Fig. 1 View of summit vents of Stromboli in January 2006 (photo by L. Lodato). Crater area ~ 300 m.

Fig. 2 Plot showing the average frequency of explosions per hour at Stromboli reported on a daily basis for the period from December 2004 to May 2006 (redrawn from plots in Stromboli weekly reports available at www.ct.ingv.it, by courtesy of A. Cristaldi). Yellow boxes mark periods with no data. Grey arrows indicate the dates of the normal explosive activity from which we collected the samples used in this study (double arrows refer to two consecutive days).

Fig. 3 a) Sketch of the tomography set up at the SYRMEP beamline at Sincrotrone Elettra and b) external (left) and internal (right) setup of the Tomolab facility, also at Sincrotrone Elettra.

Fig. 4 Examples of orthogonal views from two of the reconstructed 3-D scoria volumes from normal Strombolian activity. Cutting planes displaying inner vesicle textures indicated with abcd for both volumes. Z axis is 2.7 mm for both images.

Fig. 5 Cumulative (open circles) and non-cumulative (bars) vesicle volume distributions of the investigated scoria clasts from normal Strombolian activity at Stromboli between December 2004 and May 2006. See text for further details.

Fig. 6 3-D volumes of pumice clasts from the a) 5 April 2003 and b) 15 March 2007 paroxysmal explosions of Stromboli reconstructed via X-ray computed microtomography, and related vesicle volume distributions in b) and d), respectively. Z axis 3.5 mm in a) and 1.9 mm in c).

Fig. 7 Vesicularity and vesicle number density of the investigated scoria clasts between 21 December 2004 and 17 September 2005.

Fig. 8 Relative velocity magnitudes of fluid flow in two slices of a) scoria sample 170905a, and b) pumice clast Str50403, calculated by lattice Boltzmann simulations. The colour-bar scale in each image depicts the steady state velocity magnitude at each point in the domain multiplied by 1×10^{14} when the force applied in the x-direction is 10^{-6}. The simulation in a) demonstrates high fluid flow velocity (hotter colours) through a large connecting vesicle on the left-hand side of the image; in b) fluid transport occurs at lower values (cooler colours) through smaller vesicles. The width is 2 mm for both slices.

Electronic Supplementary Material

Complete movies of relative velocity magnitudes in samples 170905a (movie a) and Str50403 (movie b) calculated by lattice Boltzmann simulations. Colour-bar scale as in Fig. 8 of the main text. Note that the single slice on the right-hand side of both movies is reversed right-to-left compared to the 3-D image on the left.

Table 1
Vesicles in scoriae from December 2004-May 2006 normal explosive activity on Stromboli

Sample	[a]Volume (mm^3)	Vesicularity	[b]VND per mm^3	[c]VND_{melt} per mm^3	exponent
211204a1	6.0	0.31	$0.70x10^2$	$1.01x10^2$	1.14
211204a2	4.0	0.46	$0.61x10^2$	$1.13x10^2$	0.95
211204a3	2.0	0.25	nd	nd	nd
90105a1*	13.8	0.46	$1.60x10^2$	$2.96x10^2$	0.94
90105a2*	21.6	0.55	$1.80x10^2$	$4.00x10^2$	1.11
90105a3	92.5	0.57	nd	nd	nd
90105b1*	13.9	0.78	$1.00x10^2$	$4.55x10^2$	1.17
90105b2*	11.5	0.68	$1.20x10^2$	$3.75x10^2$	1.25
100205a1*	8.8	0.32	$0.76x10^2$	$1.12x10^2$	0.77
100205a2*	11.9	0.39	$0.85x10^2$	$1.39x10^2$	0.94
100205b1*	10.0	0.29	$0.98x10^2$	$1.38x10^2$	0.99
100205b2	5.8	0.32	nd	nd	nd
30305a1*	47.7	0.50	$0.60x10^2$	$1.20x10^2$	1.13
30305a2*	35.0	0.51	$1.10x10^2$	$2.24x10^2$	1.16
30305b1	13.2	0.36	nd	nd	nd
30305b2*	15.4	0.47	$0.86x10^2$	$1.62x10^2$	1.0
220505a*	34.7	0.48	$0.50x10^2$	$0.96x10^2$	0.66
170905a*	29.3	0.62	$0.80x10^2$	$2.11x10^2$	1.10
170905c2*	26.1	0.56	$0.50x10^2$	$1.14x10^2$	1.13
220506a	7.8	0.24	$0.78x10^2$	$1.03x10^2$	0.94
220506d	5.4	0.63	nd	nd	nd
240506b	9.9	0.49	$0.90x10^2$	$1.96x10^2$	0.97
Str50403*	15.7	0.58	$2.70x10^2$	$6.43x10^2$	1.40
Str150307	1.6	0.57	$3.76x10^2$	$8.60x10^2$	1.40

[a]Sample volume.
[b]Vesicle number density.
[c]Vesicle number density per melt volume.
*Asterisks indicate samples whose vesicularity comes from *Polacci et al.* [2007].
In sample labels, different letters indicate different samples; different numbers next to the same letter indicate distinct sub-volumes of the same sample. Str50403 and Str150307 are pumice clasts from paroxysmal explosions.
nd stays for not determined.

Table 2
Permeability calculations using lattice Boltzmann simulations of fluid flow

Sample	[a]L	[b]X (m^2)	[b]Y (m^2)	[b]Z (m^2)	[c]Average (m^2)
30305a1	140	$0.2x10^{-10}$	$2.2x10^{-10}$	$3.5x10^{-10}$	$2.0x10^{-10}$
170905a	140	$4.4x10^{-10}$	$8.9x10^{-10}$	$8.6x10^{-10}$	$7.3x10^{-10}$
170905c2	180	$3.6x10^{-10}$	$6.5x10^{-10}$	$3.7x10^{-10}$	$4.6x10^{-10}$
240506b	160	$16.x10^{-10}$	$0.017x10^{-10}$	$3.5x10^{-10}$	$6.5x10^{-10}$
Str50403	142	$2.7x10^{-11}$	$1.3x10^{-11}$	$2.2x10^{-11}$	$2.1x10^{-11}$
Str150307	160	$8.7x10^{-11}$	$9.1x10^{-11}$	$8.2x10^{-11}$	$8.6x10^{-11}$

[a]Edge length in pixels of the cropped tomographic volumes.
[b]Permeability values on the x, y, z directions.
[c]Permeability values averaged on the 3 (x, y, z) directions.


N

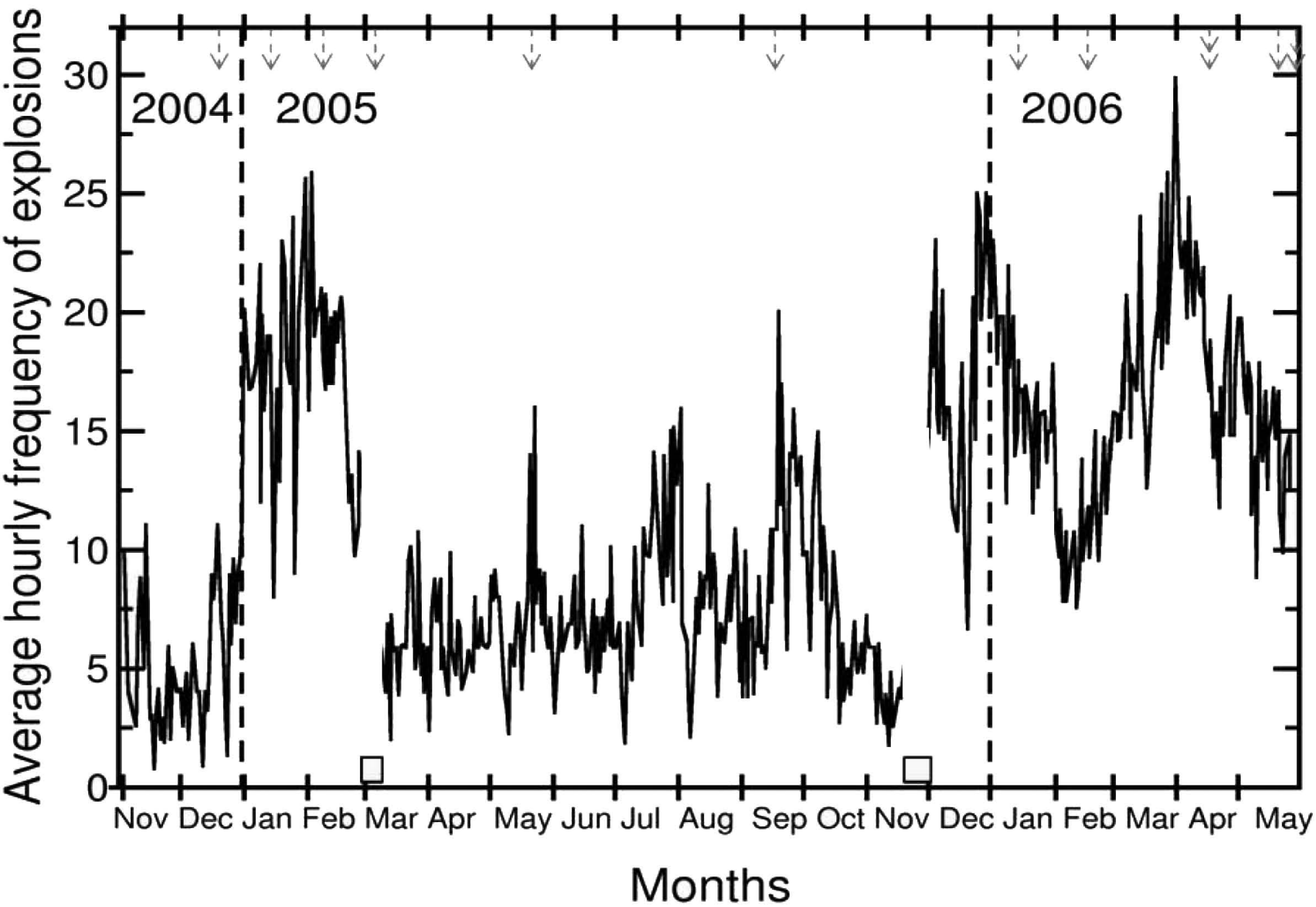
Average hourly frequency of explosions
0
5
10
15
20
25
30
2004
2005
2006
Nov Dec Jan Feb Mar Apr May Jun Jul Aug Sep Oct Nov Dec Jan Feb Mar Apr May
Months

a)

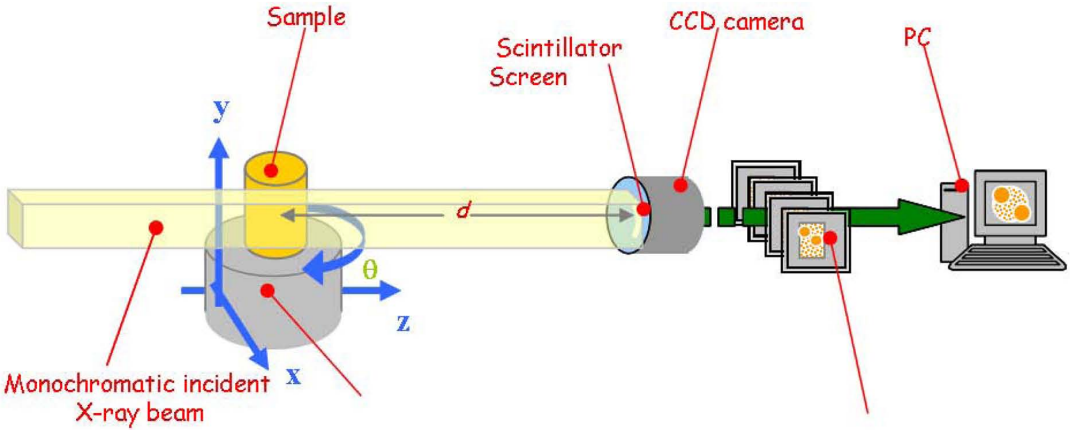
Sample
Scintillator
Screen
CCD camera
PC
y
d
θ
z
x
Monochromatic incident
X-ray beam

b)


TOMOLAB
TOMOLAB

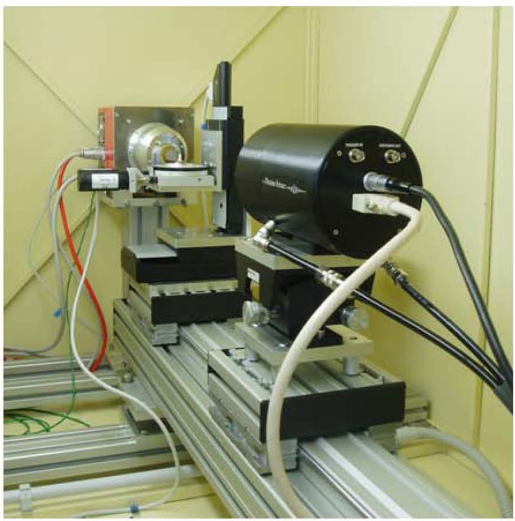

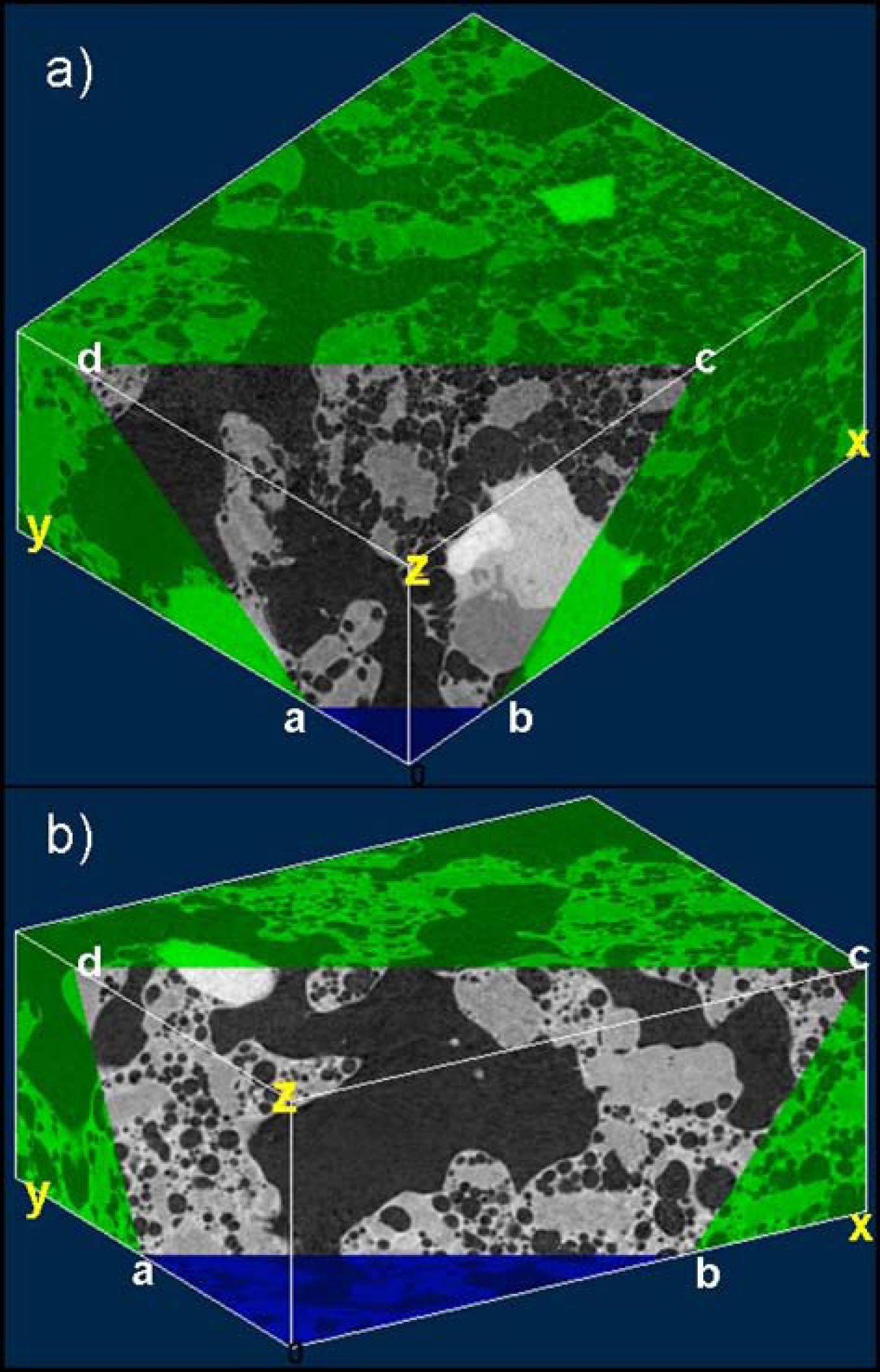
a)
d
c
x
y
z
a
b
0
b)
d
c
z
y
x
a
b
0

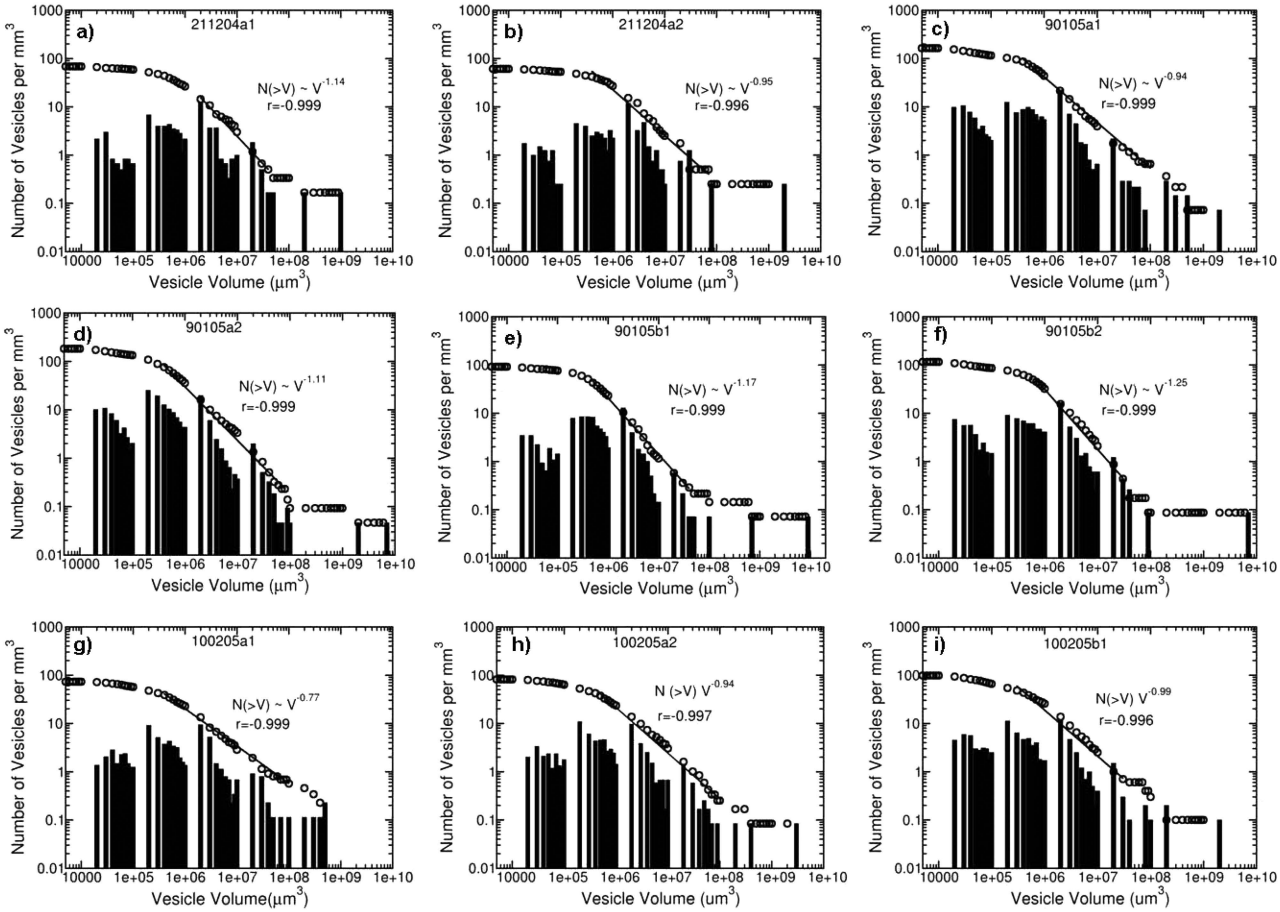
a)
211204a1
N(>V) ~ V^-1.14
r=-0.999
b)
211204a2
N(>V) ~ V^-0.95
r=-0.996
c)
90105a1
N(>V) ~ V^-0.94
r=-0.999
d)
90105a2
N(>V) ~ V^-1.11
r=-0.999
e)
90105b1
N(>V) ~ V^-1.17
r=-0.999
f)
90105b2
N(>V) ~ V^-1.25
r=-0.999
g)
100205a1
N(>V) ~ V^-0.77
r=-0.999
h)
100205a2
N (>V) V^-0.94
r=-0.997
i)
100205b1
N(>V) V^-0.99
r=-0.996
Number of Vesicles per mm3
Vesicle Volume (μm3)
Vesicle Volume(μm3)
Vesicle Volume (um3)
10000
1e+05
1e+06
1e+07
1e+08
1e+09
1e+10
0.01
0.1
1
10
100
1000

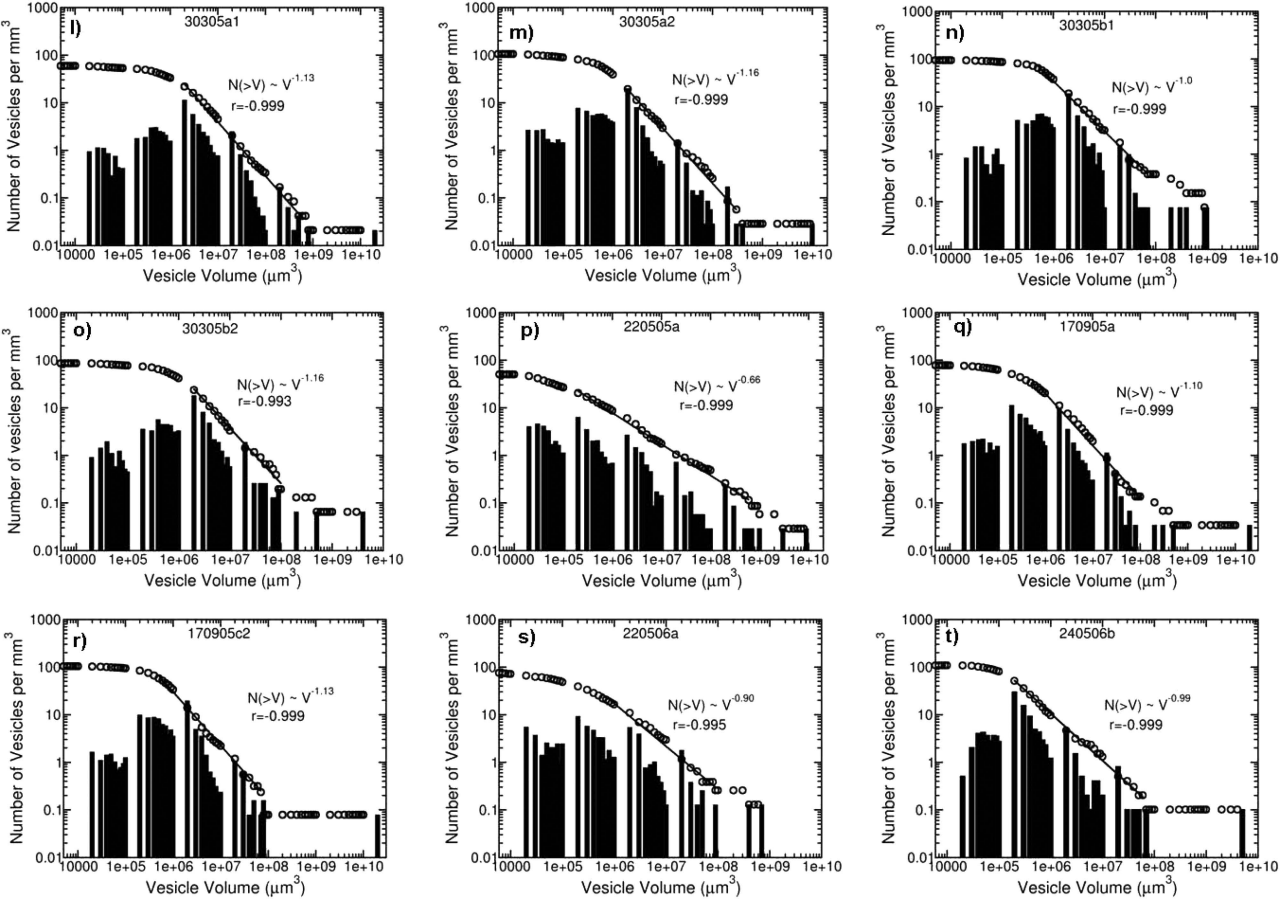
l)
30305a1
N(>V) ~ V^-1.13
r=-0.999
m)
30305a2
N(>V) ~ V^-1.16
r=-0.999
n)
30305b1
N(>V) ~ V^-1.0
r=-0.999
o)
30305b2
N(>V) ~ V^-1.16
r=-0.993
p)
220505a
N(>V) ~ V^-0.66
r=-0.999
q)
170905a
N(>V) ~ V^-1.10
r=-0.999
r)
170905c2
N(>V) ~ V^-1.13
r=-0.999
s)
220506a
N(>V) ~ V^-0.90
r=-0.995
t)
240506b
N(>V) ~ V^-0.99
r=-0.999
Number of Vesicles per mm3
Vesicle Volume (μm3)
10000 1e+05 1e+06 1e+07 1e+08 1e+09 1e+10
0.01 0.1 1 10 100 1000

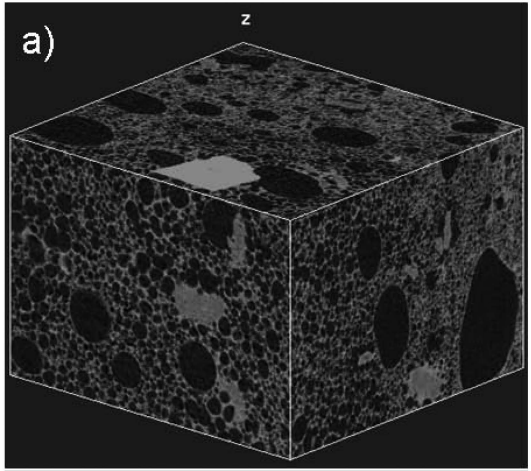
a)
z

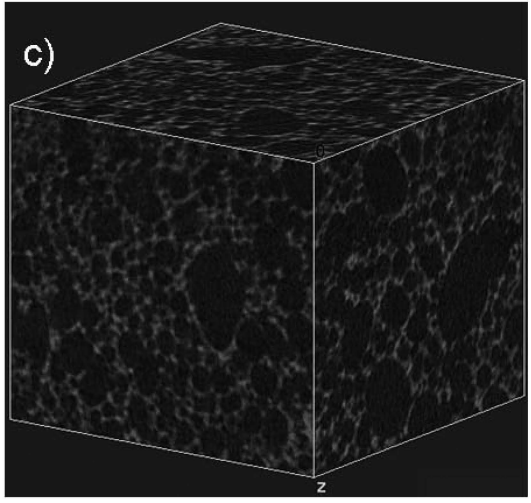
c)
z

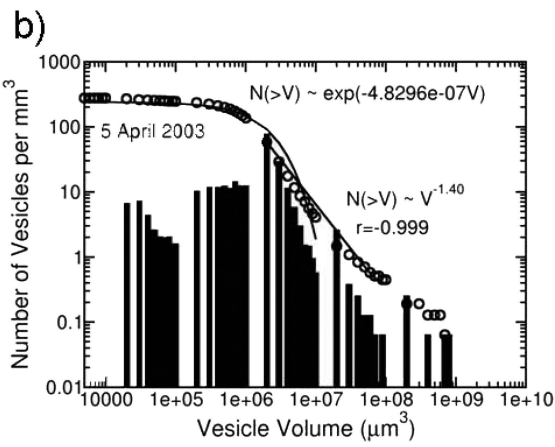
b)
N(>V) ~ exp(-4.8296e-07V)
5 April 2003
N(>V) ~ V-1.40
r=-0.999
Number of Vesicles per mm3
Vesicle Volume (μm3)
1000
100
10
1
0.1
0.01
10000
1e+05
1e+06
1e+07
1e+08
1e+09
1e+10

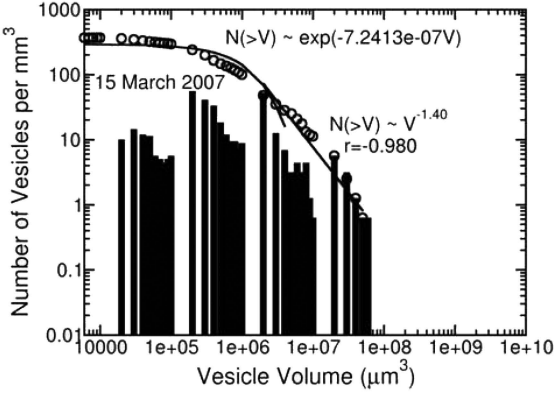
d)
N(>V) ~ exp(-7.2413e-07V)
15 March 2007
N(>V) ~ V-1.40
r=-0.980
Number of Vesicles per mm3
Vesicle Volume (μm3)
1000
100
10
1
0.1
0.01
10000
1e+05
1e+06
1e+07
1e+08
1e+09
1e+10

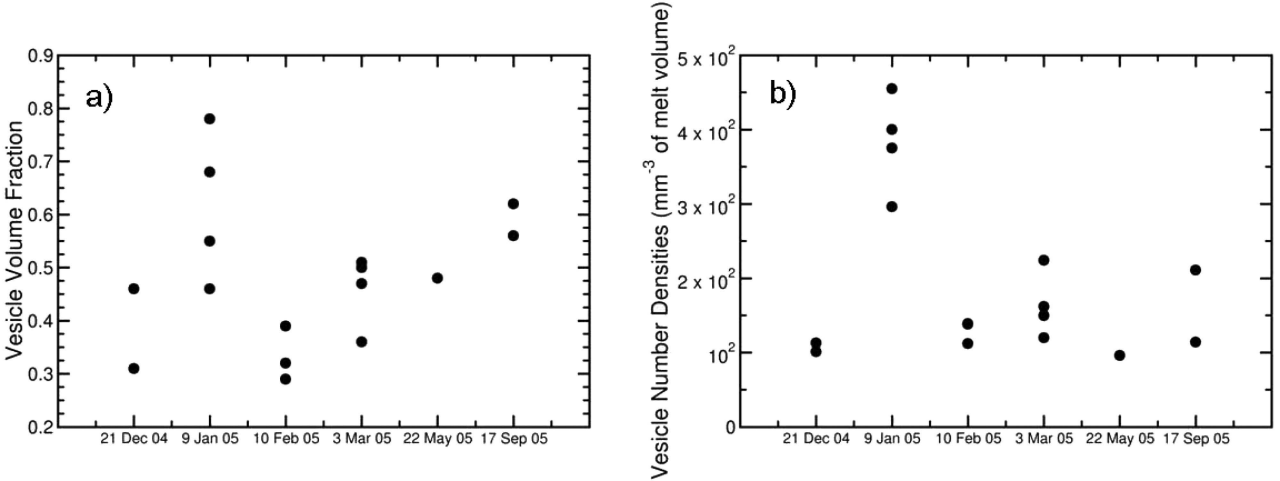
a)
Vesicle Volume Fraction
0.9
0.8
0.7
0.6
0.5
0.4
0.3
0.2
21 Dec 04
9 Jan 05
10 Feb 05
3 Mar 05
22 May 05
17 Sep 05
b)
Vesicle Number Densities (mm-3 of melt volume)
5 x 10^2
4 x 10^2
3 x 10^2
2 x 10^2
10^2
0
21 Dec 04
9 Jan 05
10 Feb 05
3 Mar 05
22 May 05
17 Sep 05

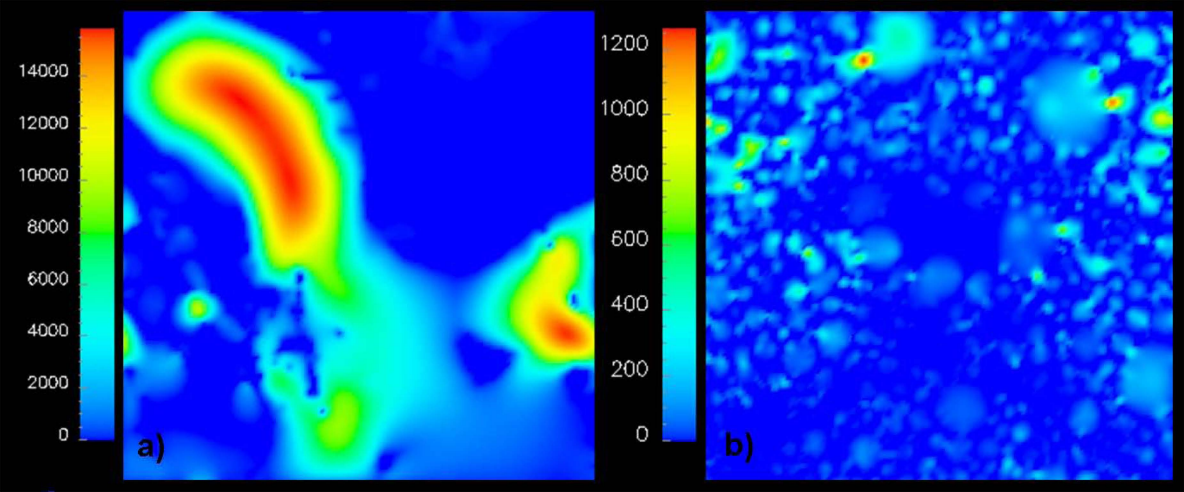
14000
12000
10000
8000
6000
4000
2000
0
a)
1200
1000
800
600
400
200
0
b)